RSC Advances

PAPER

View Article Online
View Journal | View Issue

Cite this: *RSC Adv.*, 2022, **12**, 13797

Mechanofluorochromism of (D–π–)$_2$A-type azine-based fluorescent dyes†

Kosuke Takemura, Keiichi Imato and Yousuke Ooyama *

Bathochromic or hypsochromic shift-type mechanofluorochromism (b-MFC or h-MFC) was found for (D–π–)$_2$A-type azine-based fluorescent dyes **OUY-2**, **OUK-2**, and **OUJ-2** possessing intramolecular charge-transfer (ICT) characteristics from two (diphenylamino)carbazole–thiophene units as D (electron-donating group)–π (π-conjugated bridge) moieties to a pyridine, pyrazine, or triazine ring as A (electron-withdrawing group): grinding of the recrystallized dyes induced red or blue shifts of the fluorescent colors, that is, bathochromic or hypsochromic shifts of the fluorescence maximum wavelengths ($\lambda^{\text{fl-solid}}_{\text{max}}$). The degrees of MFC evaluated by the absolute value of differences ($\Delta\lambda^{\text{fl-solid}}_{\text{max}}$) in $\lambda^{\text{fl-solid}}_{\text{max}}$ before and after grinding of the recrystallized dyes increased in the order of **OUY-2** (+7 nm) < **OUK-2** (−17 nm) < **OUJ-2** (+45 nm), so that **OUJ-2** exhibits obvious b-MFC, but **OUK-2** exhibits h-MFC. X-ray powder diffraction (XRD) and differential scanning calorimetry (DSC) demonstrated that the recrystallized dyes were in the crystalline state but the ground dyes were in the amorphous state. When the ground solids were heated above their crystallization temperatures (T_c), the colors and fluorescent colors recovered to the original ones before grinding or converted to other ones, that is, heating the ground solids in the amorphous state induced the recrystallization to recover the original microcrystals or to form other microcrystals due to polymorph transformation. However, (D–π–)$_2$Ph-type fluorescent dye **OTK-2** having a phenyl group as a substitute for the azine rings exhibited non-obvious MFC. Molecular orbital (MO) calculations indicated that the values of the dipole moments (μ_g) in the ground state were 4.0 debye, 1.4 debye, 3.2 debye, and 2.9 debye for **OTK-2**, **OUY-2**, **OUK-2**, and **OUJ-2**, respectively. Consequently, on the basis of experimental results and MO calculations, we have demonstrated that the MFC of the (D–π–)$_2$A-type azine-based fluorescent dyes is attributed to reversible switching between the crystalline state of the recrystallized dyes and the amorphous state of the ground dyes with changes in the intermolecular dipole–dipole and π–π interactions before and after grinding. Moreover, this work reveals that (D–π–)$_2$A fluorescent dyes possessing dipole moments of *ca.* 3 debye as well as moderate or intense ICT characteristics make it possible to activate the MFC.

Received 15th April 2022
Accepted 28th April 2022

DOI: 10.1039/d2ra02431d

rsc.li/rsc-advances

Introduction

Mechanofluorochromism (MFC) is a phenomenon that induces changes in fluorescent colors as well as colors of organic or metal complex fluorescent dyes in the solid state by external mechanical stimuli, being accompanied by reversion to the original colors and fluorescent colors by heating or exposure to solvent vapor.[1–7] In many cases, MFC is based on reversible changes in the electronic structures of dye molecules and/or intermolecular interactions between the dye molecules induced by changes in the chemical structures (cleavage and reconstruction of chemical bonds and twisting and distortion of the structures) or molecular orientation and arrangement of dye molecules, which are altered by solid-state transformation (crystal-to-crystal and crystal-to-amorphous phase transitions) by grinding and heating or exposure to solvent vapor, resulting in changes in the photoabsorption and fluorescence properties. In particular, the intermolecular MFC (inter-MFC) based on reversible changes in molecular orientation and arrangement of dye molecules is superior in durability to the intramolecular MFC (intra-MFC) based on reversible changes in the chemical structures of dye molecules by cleavage and reconstruction of chemical bonds during the grinding–heating process, and thus, the inter-MFC is expected to be applicable to rewritable photo-imaging and electroluminescence devices.[8–70] Among various types of fluorescent dyes possessing the mechanofluorochromic properties, donor–π–acceptor (D–π–A)-type fluorescent dyes composed of an electron-donating moiety (D) and an electron-withdrawing moiety (A) connected by a π-conjugated bridge exhibit intense photoabsorption and fluorescence emission properties based on the intramolecular charge transfer (ICT)

Applied Chemistry Program, Graduate School of Advanced Science and Engineering, Hiroshima University, 1-4-1 Kagamiyama, Higashi-Hiroshima 739-8527, Japan. E-mail: yooyama@hiroshima-u.ac.jp

† Electronic supplementary information (ESI) available. See https://doi.org/10.1039/d2ra02431d

excitation from the D moiety to the A moiety.[11–33] Thus, the dipole moments as well as photoabsorption (*i.e.*, color) and fluorescence emission (*i.e.*, fluorescent color) wavelengths of D–π–A-type fluorescent dyes are tunable by not only the electron-donating ability of D and the electron-withdrawing ability of A but also the electronic characteristics of the π-conjugated bridge. The D–π–A-type fluorescent dyes are well known to undergo significant fluorescence quenching (*i.e.*, ACQ: aggregation-caused quenching) and bathochromic shifts of the photoabsoprtion and fluorescence maximum wavelengths (λ_{max}^{abs} and λ_{max}^{fl}) from the solution to the solid state due to the delocalization of excitons or excimers by the formation of intermolecular π–π interactions between the dye molecules in the solid state, which can be controlled by changing the steric hindrance of substituents on the D and A moieties and/or π-conjugated bridge.[11–16,71–73] Therefore, the D–π–A-type fluorescent dyes occasionally show the intra-MFC based on the twisting and distortion between the π-conjugated bridge and D or A moiety or the inter-MFC based on changes in the intermolecular dipole–dipole and π–π interactions between the dye molecules. Most D–π–A-type mechanofluorochromic dyes developed so far exhibit bathochromic shift-type MFC (b-MFC): grinding of the recrystallized dyes induces red shifts of the fluorescent colors, that is, bathochromic shifts of λ_{max}^{fl}. Indeed, in our previous study, we have reported that newly developed heteropolycyclic D–π–A-type fluorescent dyes possessing moderate dipole moments (μ_g = *ca.* 5–6 debye) in the ground state show distinguished inter-b-MFC (Fig. 1a).[6,11–13] Our work revealed that the inter-b-MFC of the D–π–A-type fluorescent dyes is attributed to reversible switching between the crystalline and amorphous states with changes in intermolecular dipole–dipole and π–π interactions between the dye molecules (Fig. 1b). Meanwhile, it was found that D–π–A-type fluorescent dyes possessing large dipole moments (μ_g = *ca.* 8 debye) show weak MFC due to the strong dipole–dipole interactions between the dye molecules, changes in which may be inhibited in the crystal-to-amorphous phase transition.[14] Moreover, it was suggested that negligible MFC observed in D–π–A-type fluorescent dyes possessing small dipole moments (μ_g = *ca.* 1–2 debye) is ascribable to small changes in the dipole–dipole interactions between the crystalline and amorphous states.[15] Consequently, we proposed that the most important point for developing MFC dyes is to design D–π–A-type fluorescent dye molecules possessing moderate dipole moments (*ca.* 5 debye), which are precisely controlled by tuning the electron-donating ability of D, electron-withdrawing ability of A, steric size of substituents, and D–π–A system (Fig. 1c).[6] In addition, for the relationship between μ_g and MFC, Zhang *et al.* have reported that tetraphenylethylene (TPE) derivatives possessing large dipole moments are closely packed in the amorphous phase due to their intense ICT characteristics and the strong dipole–dipole interactions and the ICT characteristics are enhanced by grinding due to the increased molecular planarity, resulting in pronounced b-MFC.[34] In contrast, TPE derivatives possessing small dipole moments show non-obvious MFC due to their weak ICT characteristics and dipole–dipole interactions. Recently, Thomas III *et al.* have investigated the MFC of D–π–A-type phenylene ethynylenes (PEs).[17–20] They demonstrated that PEs having a strong D group exhibit b-MFC due to the formation of planarized/aggregated PEs by grinding, whereas PEs having a relatively weak D group exhibit hypsochromic shift-type MFC (h-MFC) due to the disruption of PE aggregates by grinding. Indeed, Misra *et al.* have reviewed D–A-type fluorescent dyes exhibiting h-MFC, such as triphenylamine-, TPE-, and benzothiadiazole-based derivatives.[7] Meanwhile, Yamanoi *et al.* have reported that disilane-bridged D–A–D triad composed of phenothiazine and thienopyrazine exhibits b-MFC based on changes in conformational relaxation due to the flexibility of the Si–Si bond and phenothiazine groups between the crystalline and amorphous states.[74] Therefore, in order to achieve pronounced and desired MFC that can control fluorescence properties by external mechanical stimuli, it is necessary to provide a direction in the molecular design toward creating mechanofluorochromic dyes to meet the above requirements.

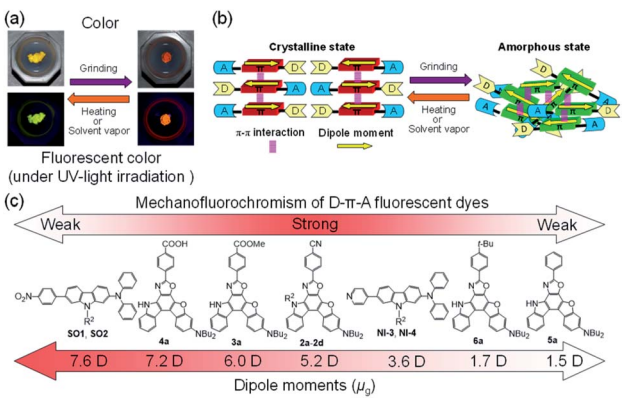

Fig. 1 (a) Photographs of powder of heteropolycyclic D–π–A fluorescent dye under room light (top) and under UV-light irradiation (down) before and after grinding and after heating the ground solid. (b) Mechanisms of MFC observed in heteropolycyclic D–π–A fluorescent dyes. (c) Correlation between dipole moments and MFC characteristics of D–π–A fluorescent dyes.

Thus, in this work, in order to further gain insight into the development of D–π–A-type mechnofluorochromic dyes, we have designed and synthesized $(D–π–)_2$A-type azine-based fluorescent dyes **OUY-2**, **OUK-2**, and **OUJ-2** with two (diphenylamino)carbazole–thiophene units as the D–π moiety and a pyridine, pyrazine, or triazine ring as the A group[75] and a $(D–π–)_2$Ph fluorescent dye **OTK-2** having a phenyl (Ph) group as a substitute for the azine rings (Fig. 2). The $(D–π–)_2$A-type fluorescent dyes are expected to show obvious MFC, that is, high fluorescent color contrast before and after grinding, because they generally exhibit high molar extinction coefficient and fluorescence quantum yield due to the intense ICT characteristics, compared with D–π–A-type fluorescent dyes. The presence or absence of MFC has been investigated from the photoabsorption, fluorescence excitation, and fluorescence spectral measurements, time-resolved fluorescence spectroscopy, X-ray powder diffraction (XRD), differential scanning calorimetry (DSC), and density measurements of the solids before and after grinding and after heating the ground solids.

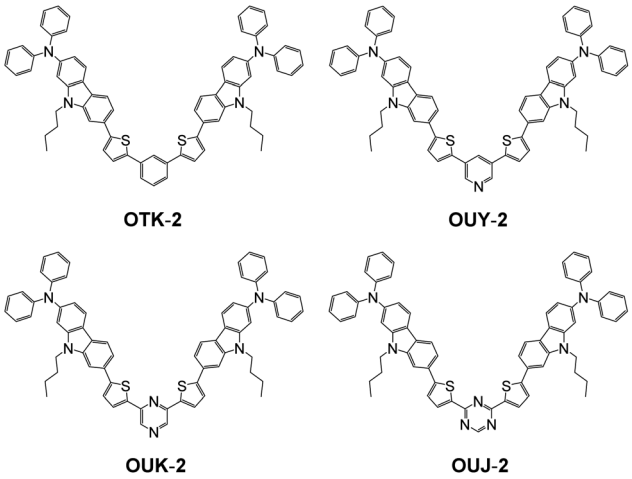

Fig. 2 Chemical structures of $(D-\pi-)_2$Ph fluorescent dye **OTK-2** and $(D-\pi-)_2$A-type azine-based fluorescent dyes **OUY-2**, **OUK-2**, and **OUJ-2**.

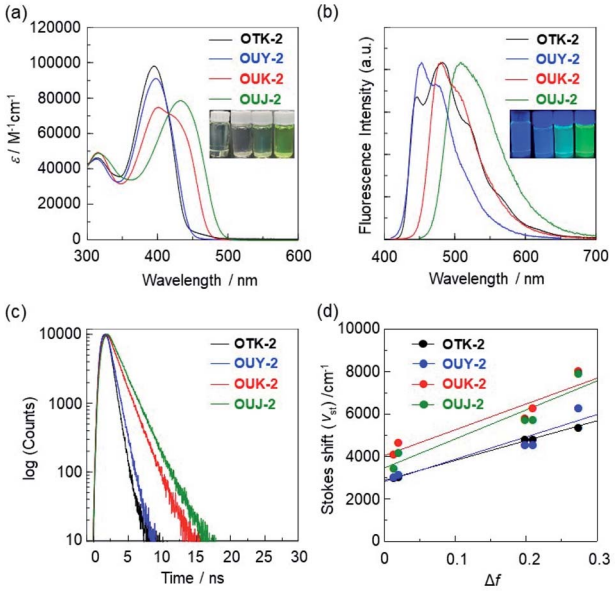

Fig. 3 (a) Photoabsorption and (b) fluorescence ($\lambda^{ex} = \lambda^{abs}_{max}$) spectra and (c) fluorescence decay profiles of **OTK-2**, **OUY-2**, **OUK-2**, and **OUJ-2** in toluene. (d) Lippert–Mataga plots of the Stokes shifts (ν_{st}) *versus* orientation polarizabilities of solvents (Δf; 0.0132 for toluene, 0.0205 for 1,4-dioxane, 0.199 for ethyl acetate, 0.2096 for THF, and 0.274 for DMF). The slopes (m_{sl}) became steep in the order of **OTK-2** (9339 cm^{-1}) < **OUY-2** (10 500 cm^{-1}) < **OUK-2** (12 200 cm^{-1}) < **OUJ-2** (13 700 cm^{-1}). The correlation coefficient (R^2) values for the calibration curves are 0.99 for **OTK-2**, 0.90 for **OUY-2**, 0.88 for **OUK-2**, and 0.89 for **OUJ-2** and indicate good linearity. Insets in (a) and (b): color and fluorescence images of **OTK-2**, **OUY-2**, **OUK-2**, and **OUJ-2** (from left) in toluene.

The MFC of $(D-\pi-)_2$A-type azine-based fluorescent dyes were estimated from the viewpoint of the degree of μ_g based on molecular orbital (MO) calculations and changes in the intermolecular dipole–dipole and π–π interactions before and after grinding. Herein we reveal the effect of μ_g of $(D-\pi-)_2$A-type fluorescent dyes on the MFC and propose the direction in molecular design toward creating D–π–A-type mechnofluorochromic dyes.

Results and discussion

The $(D-\pi-)_2$A-type azine-based fluorescent dyes **OUY-2**, **OUK-2**, and **OUJ-2** were synthesized according to a stepwise synthetic protocol that has been reported elsewhere.[75] In a similar way to **OUY-2**, **OUK-2**, and **OUJ-2**, the $(D-\pi-)_2$Ph fluorescent dye **OTK-2** was prepared by Stille coupling of a stannyl thiophene derivative having a (diphenylamino)carbazole moiety with 1,3-diiodobenzene (see Scheme S1 for the synthesis, ESI†).

In our previous work, we demonstrated that **OUY-2**, **OUK-2**, and **OUJ-2** exhibited an ICT-based photoabsorption band (λ^{abs}_{max}), which appeared in a longer wavelength region in the order of **OUY-2** < **OUK-2** < **OUJ-2** in solution, in agreement with the increase in the electron-withdrawing ability of the azine rings in the order of pyridyl group < pyrazyl group < triazyl group (Fig. 3a and Tables 1, S2†).[75] Interestingly, the photoabsorption spectra of **OUK-2** show a shoulder band in the long-wavelength region close to the λ^{abs}_{max} of **OUJ-2**. In toluene, **OUY-2** and **OUK-2** exhibited a vibronically-structured fluorescence band, while a broad fluorescence band was observed in **OUJ-2** (Fig. 3b). Moreover, the three $(D-\pi-)_2$A-type fluorescent dyes showed positive solvatofluorochromism (p-SFC): their photoabsorption spectra were nearly independent of solvent polarity, while their fluorescence spectra were dependent on solvent polarity, leading to bathochromic shifts of the fluorescence bands with increasing solvent polarity from toluene to DMF (Fig. S2†). **OUK-2** and **OUJ-2** exhibited significant SFC, that is, significant decreases in the fluorescence quantum yields (Φ_{fl}) in polar solvents such as DMF compared with **OUY-2** (Table S1†). The relationships between the λ^{fl}_{max} and solvent polarity parameters were investigated on the basis of the Lippert–Mataga equation.[76–78] The Lippert–Mataga plots of the Stokes shifts (ν_{st}) *versus* the orientation polarizabilities (Δf) of solvents revealed that the change in dipole moment, $\Delta\mu = \mu_e - \mu_g$, between the ground ($\mu_g$) and excited ($\mu_e$) states increased in the order of **OUY-2** (22 debye) < **OUK-2** (25 debye) < **OUJ-2** (26 debye), which corresponds to the increase in the electron-withdrawing ability of the azine rings (pyridyl group < pyrazyl group < triazyl group (Fig. 3d)). This result indicates that for **OUY-2**, **OUK-2**, and **OUJ-2**, the solvent-dependent bathochromic shifts in the

Table 1 Optical data of **OTK-2**, **OUY-2**, **OUK-2**, and **OUJ-2** in toluene

Dye	λ^{abs}_{max}/nm (ε_{max}/M^{-1} cm^{-1})	λ^{fl}_{max}/nm (Φ_{fl})[a]	SS[b]/cm^{-1}	τ_{fl}[c]/ns
OTK-2	395 (98 000)	447, 483 (0.36)	2945	0.62
OUY-2	398 (91 100)	453, 473 (0.38)	3051	0.82
OUK-2	401 (74 800)	480 (0.48)	4104	1.60
OUJ-2	433 (78 500)	509 (0.81)	3448	1.92

[a] Fluorescence quantum yields (Φ_{fl}) were determined by using a calibrated integrating sphere system ($\lambda^{ex} = \lambda^{abs}_{max}$). [b] Stokes shift. [c] Fluorescence lifetime.

fluorescence bands are mainly attributed to the dipole–dipole interactions between the fluorescent dye molecules and solvent molecules.[79–84] For the case of **OTK-2**, meanwhile, the photoabsorption properties (λ_{max}^{abs} and the molar extinction coefficient (ε_{max})) were nearly independent of solvent polarity as with the case of **OUY-2**, **OUK-2**, and **OUJ-2**, while the fluorescence properties (λ_{max}^{fl} and Φ_{fl}) were slightly affected by solvent polarity, resulting in weak SFC (Fig. S2 and Table S1†). The ICT-based photoabsorption and fluorescence bands of **OTK-2** appeared in a shorter wavelength region than those of **OUY-2**, **OUK-2**, and **OUJ-2** (Fig. 3), and **OTK-2** exhibited a vibronic-structured fluorescence band in solvents except for DMF, due to the lack of electron-withdrawing ability of the phenyl group. In fact, the Lippert–Mataga plots demonstrated that the $\Delta\mu$ value (21 D) of **OTK-2** was much smaller than those of **OUY-2**, **OUK-2**, and **OUJ-2** (Fig. 3d). The time-resolved fluorescence spectroscopy demonstrated that the fluorescence lifetimes (τ_{fl}) in toluene increased in the order of **OTK-2** (0.62 ns) < **OUY-2** (0.82 ns) < **OUK-2** (1.60 ns) < **OUJ-2** (1.92 ns) (Fig. 3c and Table 1). It was also found that for the four fluorescent dyes, the τ_{fl} values decreased with increasing solvent polarity from toluene to DMF (0.62–1.07 ns for **OTK-2**, 0.82–2.33 ns for **OUY-2**, 1.60–2.14 ns for **OUK-2** and 1.92–2.93 ns for **OUJ-2**, respectively, Table S1†). Consequently, the fact indicates that **OUK-2** and **OUJ-2** show salient SFC attributed to the moderate and intense ICT characteristics, respectively, due to the moderate and strong electron-withdrawing ability of the pyrazine and triazine rings, respectively. As shown in insets of Fig. 3a and b, in toluene, the colors are nearly-colorless for **OTK-2** and **OUY-2** and greenish-yellow for **OUK-2** and **OUJ-2**, and the fluorescent colors are blue for **OUY-2** and **OTK-2**, light blue for **OUK-2**, and green for **OUJ-2**.

The semi-empirical molecular orbital (MO) calculations (PM5, INDO/S method) showed that the calculated dihedral angles between the thiophene ring and carbazole skeleton were 44.1° for **OTK-2**, 44.5° for **OUY-2**, 43.6° for **OUK-2**, and 43.3° for **OUJ-2**, which were similar to each other (Fig. 4). On the other hand, the calculated dihedral angles between the thiophene ring and benzene or azine ring were 42.7° for **OTK-2**, 41.7° for **OUY-2**, 23.3° for **OUK-2**, and 1.3° for **OUJ-2**. The fact is not surprising since for **OTK-2** and **OUY-2**, the two rings were expected to greatly twist due to the steric hindrance between the hydrogen atoms of the benzene or pyridine ring and hydrogen and sulfur atoms of the thiophene ring, while for **OUK-2**, the lack of steric hindrance between the hydrogen atom of the pyrazine ring and sulfur atom of the thiophene ring would lead to the relatively small dihedral angle. On the other hand, there is no such steric hindrance for **OUJ-2**, which results in the high coplanarity of the triazine ring and thiophene ring. Moreover, the MO calculations revealed that for **OUY-2**, **OUK-2**, and **OUJ-2**, the highest occupied molecular orbitals (HOMO) were mostly localized on the two (diphenylamino)carbazole moieties containing the thiophene ring, while the lowest unoccupied molecular orbitals (LUMO) were mostly localized on the thienylpyridine moiety for **OUY-2**, the thienylpyrazine moiety for **OUK-2**, and the thienyltriazine moiety for **OUJ-2** (Fig. 4a and b). On the other hand, for **OTK-2**, both the HOMO and LUMO were

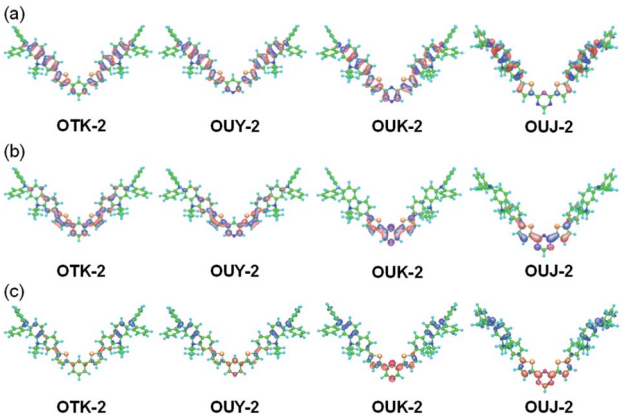

Fig. 4 (a) HOMO and (b) LUMO of OTK-2, OUY-2, OUK-2, and OUJ-2 derived from MO calculations (PM5, INDO/S method). The red and blue lobes denote the positive and negative signs of the coefficients of the molecular orbitals. The size of each lobe is proportional to the MO coefficient. (c) Calculated electron density changes accompanying the first electronic excitation of OTK-2, OUY-2, OUK-2, and OUJ-2. The blue and red lobes signify decrease and increase in electron density accompanying the electronic transition, respectively. Their areas indicate the magnitude of the electron density changes.

mostly localized on the two (diphenylamino)carbazole moieties containing the thienylbenzene moiety. The changes in the calculated electron density accompanied by the first electron excitation for the four dyes are shown in Fig. 4c, which demonstrates the ICT characteristics from the two (diphenylamino)carbazole moieties (D–π moieties) to each azine ring (A unit) upon photoexcitation. It is worth noting here that the change in the calculated electron density for **OUJ-2** is larger than those for **OUY-2** and **OUK-2**, indicating that **OUJ-2** possesses the intense ICT characteristics. The HOMO energy levels of the four dyes were similar to each other (−6.88 eV, −6.91 eV, −6.85 eV, and −7.00 eV for **OTK-2**, **OUY-2**, **OUK-2**, and **OUJ-2**, respectively), while the LUMO energy levels were lowered in the order of **OTK-2** (−0.08 eV) > **OUY-2** (−0.13 eV) > **OUK-2** (−0.40 eV) > **OUJ-2** (−0.58 eV). As the result, the HOMO–LUMO band gaps decreased in the order of **OTK-2** (6.80 eV) > **OUY-2** (6.78 eV) > **OUK-2** (6.45 eV) > **OUJ-2** (6.42 eV). Consequently, the MO calculations demonstrated that the bathochromic shifts of the ICT-based photoabsorption bands in the order of **OTK-2** < **OUY-2** < **OUK-2** < **OUJ-2** were attributed to stabilization of the LUMO energy levels due to the increase in the electron-withdrawing ability of the azine rings in the order of pyridyl group < pyrazyl group < triazyl group, as well as the increase in coplanarity of the azine or benzene ring and thiophene ring. Moreover, it was found that the values of the dipole moments (μ_g) in the ground state were 4.0 debye, 1.4 debye, 3.2 debye, and 2.9 debye for **OTK-2**, **OUY-2**, **OUK-2**, and **OUJ-2**, respectively, and keep the fact in mind because we will discuss their MFC from the viewpoint of the intermolecular dipole–dipole interactions later.

The MFC characteristics of the $(D–\pi–)_2A$ and $(D–\pi–)_2Ph$-type fluorescent dyes were investigated from the photoabsorption, fluorescence excitation, and fluorescence spectral

measurements, time-resolved fluorescence spectroscopy, X-ray powder diffraction (XRD), differential scanning calorimetry (DSC), and density measurements of the solids before and after grinding and after heating the ground solids.

First, microcrystals of **OTK-2**, **OUY-2**, **OUK-2**, and **OUJ-2** were grown by slow evaporation of the dichloromethane/*n*-hexane solutions at room temperature for several days, and then, the as-recrystallized dyes were heated at 200 °C to yield the as-prepared microcrystalline dyes for the investigation of MFC. As the result, the colors of the as-prepared dyes were yellowish orange for **OTK-2** and **OUY-2** and yellow for **OUK-2** and **OUJ-2**, and the fluorescent colors were greenish yellow for **OTK-2** and **OUJ-2**, light green for **OUY-2**, and yellow for **OUK-2** (Fig. 5). By grinding the as-prepared dyes at a stress of *ca.* 50 N cm^{-2} in a mortar with a pestle, the color and fluorescent color of the as-prepared **OUJ-2** transformed into orange. The fluorescent color of the as-prepared **OUK-2** transformed into greenish yellow by grinding, while there was no change in the color. On the other hand, the as-prepared **OTK-2** and **OUY-2** did not show obvious changes in the colors and fluorescent colors by grinding. The photoabsorption and fluorescence excitation maximum wavelengths ($\lambda_{max}^{abs\text{-}solid}$ and $\lambda_{max}^{ex\text{-}solid}$) of the as-prepared dyes appeared at 480 nm and 484 nm for **OTK-2**, 463 nm and 461 nm for **OUY-2**, 472 nm and 501 nm for **OUK-2**, and 482 nm and 477 nm for **OUJ-2**, respectively, which showed significant bathochromic shifts by 85 nm and 89 nm, 65 nm and 63 nm, 71 nm and 100 nm, and 49 nm and 44 nm, respectively, compared with those in toluene (Fig. 6–9a and b). The corresponding fluorescence maximum wavelengths ($\lambda^{fl\text{-}solid}{}_{max}$) of the as-prepared dyes appeared at 543 nm for **OTK-2**, 501 nm for **OUY-2**, 575 nm for **OUK-2**, and 545 nm for **OUJ-2**, which exhibited bathochromic shifts by 96 nm for **OTK-2**, 48 nm for **OUY-2**, 95 nm for **OUK-2**, and 36 nm for **OUJ-2**, compared with those in toluene (Fig. 6–9c). Interestingly, as with the case of the toluene solutions, the as-prepared dyes **OTK-2**, **OUY-2**, and **OUK-2** exhibited a vibronically-structured fluorescence band, whereas broad fluorescence spectra with shoulder at 527 nm and 562 nm were observed in **OUK-2** and **OUJ-2**, respectively. The fluorescence quantum yield ($\Phi_{fl\text{-}solid}$) values of the as-prepared dyes were 0.15 for **OTK-2**, 0.08 for **OUY-2**, 0.04 for **OUK-2**, and 0.12 for **OUJ-2** (Table 2), which were significantly lower than those in toluene (Table 1). The

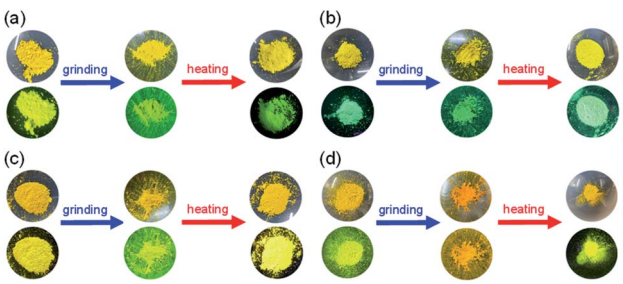

Fig. 5 Photographs of powder of (a) **OTK-2**, (b) **OUY-2**, (c) **OUK-2**, and (d) **OUJ-2** under room light (top) and under UV-light irradiation (down) before and after grinding of as-prepared microcrystalline dyes and after heating the ground solids.

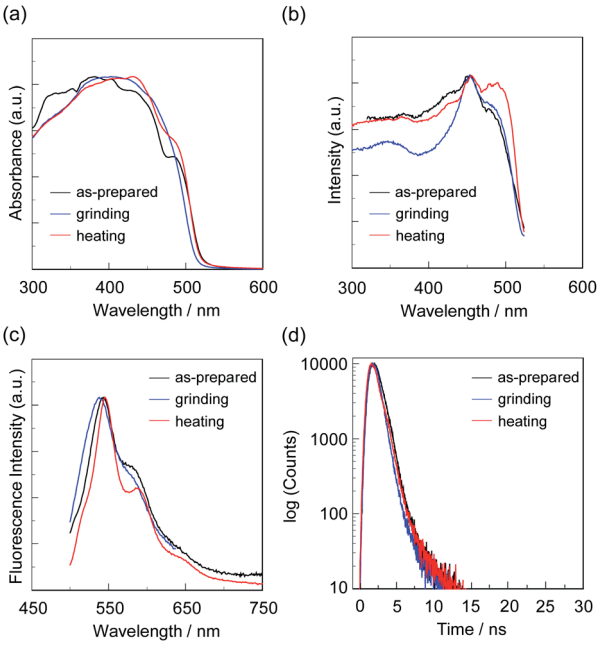

Fig. 6 (a) Solid-state UV-vis diffuse reflection–absorption, (b) fluorescence excitation at $\lambda_{max}^{fl\text{-}solid}$, and (c) fluorescence spectra ($\lambda^{ex} = \lambda_{max}^{ex\text{-}solid}$) and (d) fluorescence decay profiles of **OTK-2** before (as-prepared) and after grinding and after heating the ground solid at 200 °C.

bathochromic shifts of λ_{max}^{abs} and λ_{max}^{fl} and lowering of Φ_{fl} by changing from the solution to the solid state would be attributed to the formation of intermolecular π–π interactions

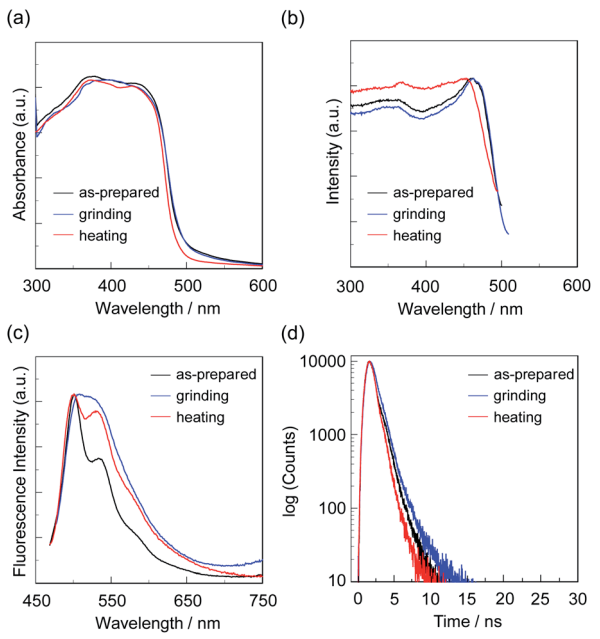

Fig. 7 (a) Solid-state UV-vis diffuse reflection–absorption, (b) fluorescence excitation at $\lambda_{max}^{fl\text{-}solid}$, and (c) fluorescence spectra ($\lambda^{ex} = \lambda_{max}^{ex\text{-}solid}$) and (d) fluorescence decay profiles of **OUY-2** before (as-prepared) and after grinding and after heating the ground solid at 200 °C.

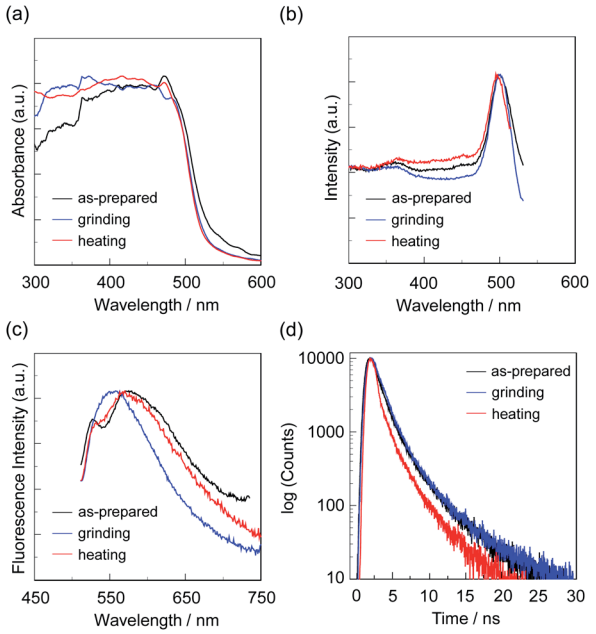

Fig. 8 (a) Solid-state UV-vis diffuse reflection–absorption, (b) fluorescence excitation at $\lambda_{max}^{fl\text{-}solid}$, and (c) fluorescence spectra ($\lambda^{ex} = \lambda_{max}^{ex\text{-}solid}$) and (d) fluorescence decay profiles of **OUK-2** before (as-prepared) and after grinding and after heating the ground solid at 180 °C.

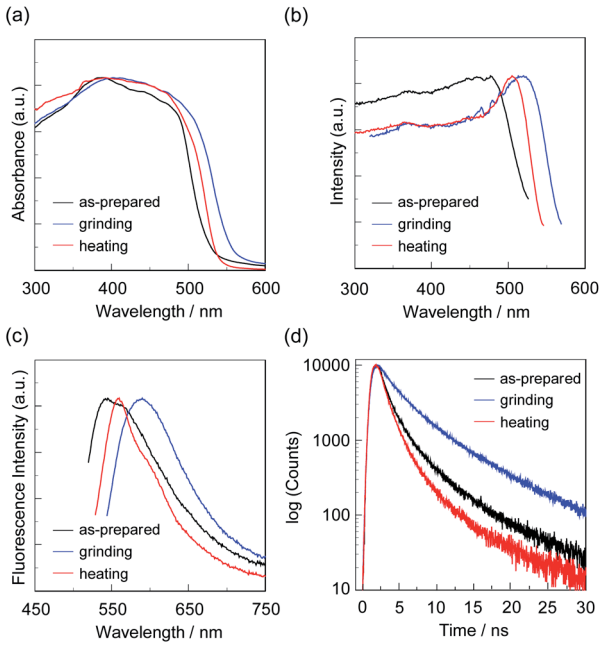

Fig. 9 (a) Solid-state UV-vis diffuse reflection–absorption, (b) fluorescence excitation at $\lambda_{max}^{fl\text{-}solid}$, and (c) fluorescence spectra ($\lambda^{ex} = \lambda_{max}^{ex\text{-}solid}$) and (d) fluorescence decay profiles of **OUJ-2** before (as-prepared) and after grinding and after heating the ground solid at 200 °C.

between the fluorophores in the solid state and consequent delocalization of excitons or excimers,[71–73] while unfortunately, we could not obtain single crystals of **OTK-2**, **OUY-2**, **OUK-2**, and **OUJ-2** with sufficient size to make the X-ray structural analysis possible. The as-prepared **OTK-2** did not exhibit any appreciable changes in the $\lambda_{max}^{abs\text{-}solid}$, $\lambda_{max}^{ex\text{-}solid}$, and $\lambda_{max}^{fl\text{-}solid}$ by grinding (Fig. 6a–c). For **OUY-2** and **OUK-2**, the $\lambda_{max}^{fl\text{-}solid}$ were red-shifted and blue-shifted, respectively, while the $\lambda_{max}^{abs\text{-}solid}$ and $\lambda_{max}^{ex\text{-}solid}$ changed little by grinding (Fig. 7a–c and 8a–c). Thus, this result revealed that **OUY-2** exhibits non-obvious b-MFC, but **OUK-2** exhibits h-MFC. For **OTK-2**, **OUY-2**, and **OUK-2**, the vibronic structures in the fluorescence bands disappeared after grinding. Compared with **OUY-2**, on the other hand, **OUJ-2** exhibited significant bathochromic shifts of the $\lambda_{max}^{abs\text{-}solid}$, $\lambda_{max}^{ex\text{-}solid}$, and $\lambda_{max}^{fl\text{-}solid}$ by grinding, that is, pronounced b-MFC (Fig. 9a–c). The degrees of MFC, which were evaluated by the absolute value of differences ($\Delta\lambda_{max}^{abs\text{-}solid}$, $\Delta\lambda_{max}^{ex\text{-}solid}$, and $\Delta\lambda_{max}^{fl\text{-}solid}$) in $\lambda_{max}^{abs\text{-}solid}$, $\lambda_{max}^{ex\text{-}solid}$, and $\lambda_{max}^{fl\text{-}solid}$ before and after grinding of the as-prepared dyes, increased in the order of **OUY-2** (n.d., n.d., −5 nm) < **OUK-2** (0 nm, +2 nm, +7 nm) ≪ **OUK-2** (+8 nm, 0 nm, −17 nm) < **OUJ-2** (+42 nm, +43 nm, +45 nm), in agreement with the order of increase in the electron-withdrawing ability of the azine rings in the order of pyridyl group < pyrazyl group < triazyl group (Table 2). On the other hand, it is worth mentioning here that the $\Delta\lambda_{max}^{fl\text{-}solid}$ between the shoulder fluorescence band of the as-prepared dyes and the $\lambda_{max}^{fl\text{-}solid}$ after grinding are +31 nm for **OUK-2** and +28 nm for **OUJ-2**, in which this can be regarded as the b-MFC of **OUK-2** as well as **OUJ-2**. The $\Phi_{fl\text{-}solid}$ values increased slightly by grinding from 0.15, 0.08, 0.04, and 0.12 to 0.16, 0.10, 0.06, and 0.17 for **OTK-2**, **OUY-2**, **OUK-2**, and **OUJ-2**, respectively (Table 2). Moreover, the time-resolved fluorescence spectroscopy revealed that the fluorescence lifetime ($\tau_{fl\text{-}solid}$) value of the as-prepared **OTK-2** became shorter from 0.93 ns before grinding to 0.73 ns after grinding, whereas the $\tau_{fl\text{-}solid}$ values of **OUY-2**, **OUK-2**, and **OUJ-2** became longer from 1.02 ns, 2.04 ns, and 2.14 ns before grinding to 1.05 ns, 2.16 ns, and 5.29 ns after grinding, respectively (Fig. 6–9d and Table 2). In particular, the $\tau_{fl\text{-}solid}$ value of **OUJ-2** after grinding were 2.5 times longer than that before grinding. When the ground solids were heated at 180–200 °C (above the recrystallization temperatures (T_c), as described later) or exposed to solvent vapor such as THF for several minutes (for **OUJ-2**, Fig. S4 and S5†), the photoabsorption, fluorescence excitation, and fluorescence bands of **OTK-2** and **OUK-2** as well as the colors and fluorescent colors recovered to the original ones before grinding, whereas the intensity of the vibronic structure in the fluorescence band of **OUY-2** and the $\lambda_{max}^{abs\text{-}solid}$, $\lambda_{max}^{ex\text{-}solid}$, and $\lambda^{fl\text{-}solid}{}_{max}$ of **OUJ-2** were different from the original ones before grinding. Besides, the fluorescence spectra of **OUJ-2**, which showed the pronounced b-MFC, after grinding and heating the ground solid were repeatedly measured several times (Fig. 10a). The fluorescence spectra showed a change in the $\lambda_{max}^{fl\text{-}solid}$ from 590 nm after grinding to 560 nm after heating. Indeed, the grinding-heating cycles indicated that **OUJ-2** exhibited good reversibility of the $\lambda_{max}^{fl\text{-}solid}$ (Fig. 10b). Meanwhile, with regard to the chemical stability of the dyes by grinding and heating, the ^{1}H NMR spectra of the samples after grinding and heating demonstrated that all the four

Table 2 Optical data of **OTK-2**, **OUY-2**, **OUK-2**, and **OUJ-2** in the solid state

Dye	$\lambda_{max}^{abs\text{-}solid}$/nm	$\Delta\lambda_{max}^{abs\text{-}solid}$/nm	$\lambda_{max}^{ex\text{-}solid}$/nm	$\Delta\lambda_{max}^{ex\text{-}solid}$/nm	$\lambda_{max}^{fl\text{-}solid}$/nm ($\Phi_{fl\text{-}solid}$)[a]	$\Delta\lambda_{max}^{fl\text{-}solid}$/nm	$\tau_{fl\text{-}solid}$[b]/ns
OTK-2 (as-prepared)	480^{shoulder}		484^{shoulder}		543 (0.15)		0.93
		—[c]		0[d]		−5[d]	
OTK-2 (grinding)	—[c]		484^{shoulder}		538 (0.16)		0.73
		—[c]		+4[e]		+7[e]	
OTK-2 (heating)	480^{shoulder}		488		545 (0.19)		0.84
OUY-2 (as-prepared)	463^{shoulder}		461		501 (0.08)		1.02
		0[d]		+2[d]		+7[d]	
OUY-2 (grinding)	463^{shoulder}		463		508 (0.10)		1.05
		−3[e]		−10[e]		−7[e]	
OUY-2 (heating)	460^{shoulder}		453		501 (0.12)		0.81
OUK-2 (as-prepared)	472		501		527^{shoulder}, 575 (0.04)		2.04
		+8[d]		0[d]		+31, −17[d]	
OUK-2 (grinding)	480^{shoulder}		501		558 (0.06)		2.16
		−8[e]		−6[e]		−31, +12[e]	
OUK-2 (heating)	472		495		527, 570 (0.04)		2.14
OUJ-2 (as-prepared)	482^{shoulder}		477		545, 562^{shoulder} (0.12)		2.14
		+42[d]		+43[d]		+45, +28[d]	
OUJ-2 (grinding)	524^{shoulder}		520		590 (0.17)		5.29
		−14[e]		−15[e]		−30[e]	
OUJ-2 (heating)	510^{shoulder}		505		560 (0.13)		1.98

[a] Fluorescence quantum yields ($\Phi_{fl\text{-}solid}$) were determined by using a calibrated integrating sphere system ($\lambda^{ex} = \lambda_{max}^{ex\text{-}solid}$). [b] Fluorescence lifetime. [c] Due to broadened band. [d] $\lambda_{max}^{abs,\ ex,\ or\ fl\text{-}solid}$ (grinding) − $\lambda_{max}^{abs,\ ex,\ or\ fl\text{-}solid}$ (as-prepared). [e] $\lambda_{max}^{abs,\ ex,\ or\ fl\text{-}solid}$ (heating) − $\lambda_{max}^{abs,\ ex,\ or\ fl\text{-}solid}$ (grinding).

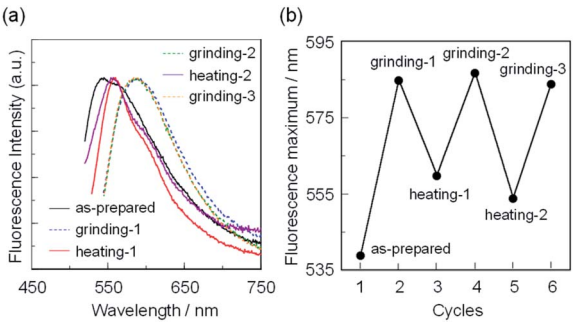

Fig. 10 (a) Solid-state fluorescence spectra ($\lambda^{ex} = \lambda_{max}^{ex\text{-}solid}$) of **OUJ-2** before (as-prepared) and after grinding and heating process. (b) Reversible switching of fluorescence maximum wavelength of **OUJ-2** during the grinding-heating process.

fluorescent dyes were not decomposed by grinding and heating (for **OUJ-2**, Fig. S3†).

The XRD measurements with the as-prepared dyes **OTK-2**, **OUY-2**, **OUK-2**, and **OUJ-2** exhibited diffraction peaks ascribable to well-defined microcrystalline structures (Fig. 11a, c, e and g). The peaks disappeared almost completely after grinding, indicating that the crystal lattices were significantly disrupted. The diffraction peaks of **OTK-2** and **OUK-2** after heating the ground solids were similar to those before grinding, that is, the as-prepared dyes, indicating recovery of the microcrystalline structures by heating. On the other hand, the XRD patterns of **OUY-2** and **OUJ-2** after heating the ground solids showed diffraction peaks at around $2\theta = 3°$ for **OUY-2** and $2\theta = 3°$, 6°, and 12° for **OUJ-2**, which were not observed in those of the as-prepared dyes. Furthermore, the DSC analysis for the four fluorescent dyes indicated that the as-prepared dyes **OUK-2** and **OUJ-2** showed only one sharp endothermic peak associated with melting (T_m) at 279 °C and 263 °C, respectively, but the DSC traces of the as-prepared dyes **OTK-2** and **OUY-2** were typical of polymorphic mixtures (Fig. 11b, d, f and h). The as-prepared dye **OTK-2** showed a T_{m1} at 249 °C and then recrystallization (T_c) at 258 °C, which in turn melted at 272 °C (T_{m2}). Interestingly, **OUY-2** has three crystal forms. The DSC traces of the as-prepared dye **OUY-2** showed a T_{m1} at 230 °C, T_{c1} at 233 °C, T_{m2} at 262 °C, T_{c2} at 269 °C, and T_{m3} at 278 °C. The MFC for crystal polymorphism of **OUY-2** will be reported elsewhere. The DSC traces of the ground solids of the four dyes were typical of amorphous solids: the ground solids underwent an endothermic glass transition (T_g) and then an exothermic T_c before T_m. It is worth noting here that by heating the ground solids in the amorphous state, **OUY-2** did not recover the original microcrystalline structure but form a more stable microcrystalline structure showing T_{m3} at 278 °C, and **OUJ-2** formed another microcrystalline structure showing T_{m2} at 268 °C, which was not observed in the DSC trace of the as-prepared microcrystal. After the ground solids of the four dyes were heated at 180–200 °C above the T_c, the DSC traces showed only one T_m for **OUY-2**, **OUK-2**, and **OUJ-2** but one T_c and two T_m for **OTK-2** due to the crystal polymorphism. Consequently, the XRD and DSC studies revealed that heating the ground solids in the amorphous state induced the recrystallization to recover the original microcrystals or to form the other microcrystals due to the polymorph transformation. Moreover, it was found that as

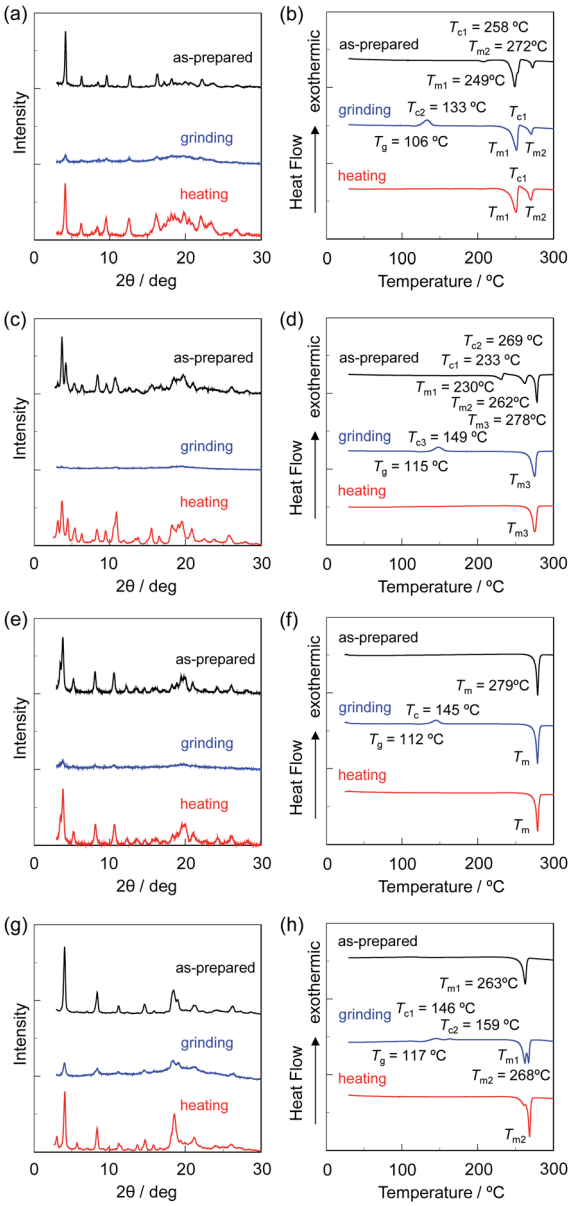

Fig. 11 XRD patterns of (a) **OTK-2**, (c) **OUY-2**, (e) **OUK-2**, and (g) **OUJ-2** and DSC curves (heating process from 25 °C to 300 °C with scan rate of 10 °C min^{-1}) of (b) **OTK-2**, (d) **OUY-2**, (f) **OUK-2**, and (h) **OUJ-2** before (as-prepared) and after grinding and after heating the ground solid.

with the case of D–π–A-type fluorescent dyes,[11–15] the MFC of the $(D–π–)_2$A-type azine-based fluorescent dyes was not just a matter of events originating from a reversible change between crystalline and amorphous states by grinding and heating, because **OUY-2** as well as **OTK-2** exhibited non-obvious MFC. More interestingly, the densities of the solids measured by the Archimedian method were found to increase by grinding from 1.40, 1.26, 1.25, and 1.13 g cm^{-3} to 1.45, 1.37, 1.39, and 1.31 g cm^{-3} for **OTK-2**, **OUY-2**, **OUK-2**, and **OUJ-2**, respectively, indicating that the dye molecules in the amorphous state after grinding were more densely packed.

On the basis of the above experimental results and MO calculations, we discuss the mechanism of MFC observed in the $(D–π–)_2$A fluorescent dyes below. In the crystalline state of the D–π–A and $(D–π–)_2$A fluorescent dyes, the long range π–π interactions between adjacent molecular planes cause the stacking of the dye molecules so as to maximize the intermolecular dipole–dipole interactions by arranging the dipole moments in anti-parallel orientation, leading to the bathochromic shifts of λ_{max}^{abs} and λ_{max}^{fl} by changing from the solution to the crystalline state. Moreover, the lowering of Φ_{fl} from the solution to the crystalline state is attributed to the delocalization of excitons due to the formation of the long-range intermolecular π–π interactions in the crystalline state, leading to a non-radiative decay route for the excited states. By grinding the as-prepared microcrystalline dyes, on the other hand, the dye molecules would move closer to each other so as to maximize the dipole–dipole interactions (so as to arrange the adjacent dipole moments in head-to-tail orientation) as well as the intermolecular π–π interactions, as evidenced by the increased densities of the dyes in the amorphous state. The dipole–dipole interaction energy will be enhanced in dyes with greater dipole moments. In fact, the μ_g values of **OUK-2** and **OUJ-2** were 3.2 debye and 2.9 debye, respectively, which were greater than 1.4 debye for **OUY-2**, reflecting that **OUK-2** and **OUJ-2** have the π-conjugated planes with the D–π moieties and strongly electron-withdrawing pyrazyl group or triazyl group, respectively. Therefore, it may be inferred that the bathochromic shifts of $\lambda_{max}^{abs\text{-}solid}$ and $\lambda_{max}^{fl\text{-}solid}$ observed in **OUJ-2** by changing from the crystalline state to the amorphous state were caused due to the strong dipole–dipole interactions, whereas the non-obvious b-MFC for **OUY-2** is ascribable to small changes in the dipole–dipole interactions between the crystalline and amorphous states due to its small dipole moment ($\mu_g = 1.4$ debye), as with the case of non-obvious MFC for D–π–A-type fluorescent dyes with small dipole moments (μ_g = *ca.* 1–2 debye) in our previous study.[15] On the other hand, it is speculated that the moderate ICT characteristics of **OUK-2** may induces the h-MFC due to the twisting and distortion between the D–π moiety and A unit by grinding, as well as apparent b-MFC due to the strong dipole–dipole interactions which was suggested by the bathochromic shift of the shoulder fluorescence band by grinding. Meanwhile, the Φ_{fl} values in the amorphous state were slightly greater than those in the crystalline state, suggesting that the short-range π–π interactions between the dye molecules in the amorphous state discouraged the delocalization of excitons unlike the case of the long-range intermolecular π–π interactions between the dye molecules in the crystalline state. Consequently, this work reveals that $(D–π–)_2$A fluorescent dyes possessing dipole moments of *ca.* 3 debye as well as ICT characteristics make it possible to activate the MFC. Moreover, it was found that a $(D–π–)_2$A structure possessing intense ICT characteristics is necessary to exhibit pronounced MFC, judging from the fact that the $(D–π–)_2$Ph fluorescent dye **OTK-2** without any electron-withdrawing moiety but with a relatively strong dipole moment ($\mu_g = 4.0$ debye) showed the non-obvious MFC. However, further fundamental studies to gain insight into the correlation between the ICT characteristics as well as the dipole moment and the MFC characteristics of $(D–π–)_2$A fluorescent dyes, that is, an investigation into MFC of $(D–π–)_2$A fluorescent dyes with dipole

moments over 3 debye, are absolutely necessary and will be reported in a subsequent paper.

Conclusions

We have found that (D–π–)$_2$A-type azine-based fluorescent dyes possessing moderate or intense intramolecular charge-transfer (ICT) characteristics exhibit hypsochromic shift-type or bathochromic shift-type mechanofluorochromism (h-MFC or b-MFC): grinding of the recrystallized dyes induces hypsochromic or bathochromic shifts of the fluorescence maximum wavelengths. The experimental results and molecular orbital (MO) calculations demonstrated that the MFC of the (D–π–)$_2$A-type azine-based fluorescent dyes was attributed to reversible switching between the crystalline state and amorphous state with changes in the intermolecular dipole–dipole and π–π interactions by grinding. We revealed that a (D–π–)$_2$A structure possessing moderate or intense ICT characteristics is necessary to exhibit pronounced MFC: (D–π–)$_2$A fluorescent dyes possessing dipole moments of *ca.* 3 debye as well as moderate or intense ICT characteristics make it possible to activate the MFC. Consequently, this work provided not only the correlation between the ICT characteristics as well as the dipole moment and MFC characteristics of (D–π–)$_2$A fluorescent dyes but also a direction in the molecular design toward creating mechanofluorochromic dyes based on the dipole moment.

Experimental

General

Melting points were measured with an AS ONE ATM-02. IR spectra were recorded on a SHIMADZU IRTracer-100 by ATR method. ^{1}H NMR and ^{13}C NMR spectra were recorded on a Varian-500 FT NMR spectrometer. High-resolution mass spectral data by APCI were acquired on a Thermo Fisher Scientific LTQ Orbitrap XL. Photoabsorption spectra of solutions were observed with a Shimadzu UV-3600 plus spectrophotometer. Photoabsorption spectra of solids were recorded by a Shimadzu UV-3600 plus spectrophotometer with a calibrated integrating sphere system. Fluorescence spectra of solutions and solids were measured with a HORIBA FluoroMax-4 spectrofluorometer. Fluorescence quantum yields in solution and in the solid state were determined using a HORIBA FluoroMax-4 spectrofluorometer with a calibrated integrating sphere system. Fluorescence decay measurements were performed on a HORIBA DeltaFlex modular fluorescence lifetime system using a Nano LED pulsed diode excitation source (451 nm). Powder X-ray diffraction measurements were performed on a Rigaku MiniFlex600-C/CM diffractometer with Cu Kα radiator. Differential scanning calorimetry was carried out using a Shimadzu DSC-60. Load measurements were performed with an IMADA push–pull scale & digital force gauge (ZP-200/V). Densities of solids were evaluated with a Shimadzu AUW220D electronic balance equipped with an SMK-401 saucer by the Archimedian method. Semi-empirical calculations were carried out with the WinMOPAC Ver. 3.9 package (Fujitsu, Chiba, Japan), where geometry calculations of the compounds in the ground state were made using the AM1 method. Dipole moments and HOMO and LUMO energy levels of the compounds were also evaluated from INDO/S calculations.

Conflicts of interest

There are no conflicts to declare.

Acknowledgements

This work was supported by Grant-in-Aids for Scientific Research on Innovative Areas "Soft Crystals" (No. 2903) (JSPS KAKENHI Grant No. 18H04520) and for Scientific Research (B) (JSPS KAKENHI Grant No. 19H02754) and the Murata Science Foundation.

Notes and references

1 Z. Chi, X. Zhang, B. Xu, X. Zhou, C. MA, Y. Zhang, S. Liu and J. Xu, Recent advances in organic mechanofluorochromic materials, *Chem. Soc. Rev.*, 2012, **41**, 3878–3896.
2 X. Zhang, Z. Chi, Y. Zhang, S. Liu and J. Xu, Recent advances in mechanochromic luminescent metal complexes, *J. Mater. Chem. C*, 2013, **1**, 3376–3390.
3 J. Xu and Z. Chi, *Mechanochromic Fluorescent Materials, RSC Smart Materials*, the Royal Society of Chemistry, 2014.
4 J. Zhao, Z. Chi, Z. Yang, Y. Zhang, E. Ubba and Z. Chi, Recent progress in the mechanofluorochromism of distyrylanthracene derivatives with aggregation-induced emission, *Mater. Chem. Front.*, 2018, **2**, 1595–1608.
5 J. Zhao, Z. Chi, Y. Zhang, Z. Mao, Z. Yang, E. Ubba and Z. Xhi, Recent progress in the mechanofluorochromism of cyanoethylene derivatives with aggregation-induced emission, *J. Mater. Chem. C*, 2018, **6**, 6327–6353.
6 Y. Ooyama, Mechanofluorochromism of D-π-A fluorescent dyes, *J. Synth. Org. Chem., Jpn.*, 2018, **76**, 1024–1041.
7 R. Misra, F. Khan, A. Ekbote and G. Singh, Mechanochromic luminogens with hypsochromically shifted emission switching property: Recent advances and perspectives, *J. Mater. Chem. C*, 2022, **10**, 5024–5064.
8 Y. Sagara, T. Mutai, I. Yoshikawa and K. Araki, Material design for piezochromic luminescence: hydrogen-bond-directed assemblies of a pyrene derivative, *J. Am. Chem. Soc.*, 2007, **129**, 1520–1521.
9 H. Ito, T. Saito, N. Oshima, N. Kitamura, S. Ishizaka, Y. Hinatsu, M. Wakeshima, M. Kato, K. Tsuge and M. Sawamura, Reversible mechanochromic luminescence of [$(C_6F_5Au)_2$(μ-1,4-diisocyanobenzene)], *J. Am. Chem. Soc.*, 2008, **130**, 10044–10045.
10 M. Tanioka, S. Kamino, A. Muranaka, Y. Ooyama, H. Ota, Y. Shirasaki, J. Horigome, M. Ueda, M. Uchiyama, D. Sawada and S. Enomoto, Reversible near-infrared/blue mechanofluorochromism of aminobenzopyranoxanthene, *J. Am. Chem. Soc.*, 2015, **137**, 6436–6439.
11 Y. Ooyama, Y. Kagawa, H. Fukuoka, G. Ito and Y. Harima, Mechanofluorochromism of a series of benzofuro[2,3-*c*]

oxazolo[4,5-*a*]carbazole-type fluorescent dyes, *Eur. J. Org. Chem.*, 2009, 5321–5326.

12 Y. Ooyama and Y. Harima, Molecular design of mechanofluorochromic dyes and their solid-state fluorescence properties, *J. Mater. Chem.*, 2011, **21**, 8372–8380.

13 Y. Ooyama, G. Ito, H. Fukuoka, T. Nagano, Y. Kagawa, I. Imae, K. Komaguchi and Y. Harima, Mechanofluorochromism of heteropolycyclic donor–π-acceptor type fluorescent dyes, *Tetrahedron*, 2010, **66**, 7268–7271.

14 Y. Ooyama, T. Sugiyama, Y. Oda, Y. Hagiwara, N. Yamaguchi, E. Miyazaki, H. Fukuoka, T. Mizumo, Y. Harima and J. Ohshita, Synthesis of carbazole-type D-π-A fluorescent dyes possessing solid-state red fluorescence properties, *Eur. J. Org. Chem.*, 2012, 4853–4859.

15 Y. Ooyama, N. Yamaguchi, S. Inoue, T. Nagano, E. Miyazaki, H. Fukuoka, I. Imae, K. Komaguchi, J. Ohshita and Y. Harima, Mechanofluorochromism of carbazole-type D–π–A fluorescent dyes, *Tetrahedron*, 2012, **68**, 529–533.

16 Y. Ooyama, Y. Oda, Y. Hagiwara, H. Fukuoka, E. Miyazaki, T. Mizumo and J. Ohshita, Solid-state fluorescence properties and mechanofluorochromism of D–π-A pyridinium dyes bearing various counter anions, *Tetrahedron*, 2013, **69**, 5818–5822.

17 S. A. Sharbe, K.-C. Shih, A. Mann, F. Frausto, T. E. Hass, M.-P. Nieh and S. W. Thomas, Reversible mechanofluorochromism of aniline-terminated phenylene ethynylenes, reversible mechanofluorochromism of aniline-terminated phenylene ethynylenes, *Chem. Sci.*, 2018, **9**, 5415–5426.

18 S. A. Sharber, A. Mann, K.-C. Shih, W. J. Mullin, M.-P. Nieh and S. W. Thomas III, Directed polymorphism and mechanofluorochromism of conjugated materials through weak non-covalent control, *J. Mater. Chem. C*, 2019, **7**, 8316–8324.

19 S. A. Sharber and S. W. Thomas III, Side chain regioisomers that dictate optical properties and mechanofluorochromism through crystal packing, *Chem. Mater.*, 2020, **32**, 5785–5801.

20 S. A. Sharber, W. J. Mullin and S. W. Thomas III, Bridging the void: halogen bonding and aromatic interactions to program luminescence and electronic properties of π-conjugated materials in the solid state, *Chem. Mater.*, 2021, **33**, 6640–6661.

21 H. Sun, Y. Zhang, W. Yan, W. Chen, Q. Lan, S. Liu, L. Jiang, Z. Chi, X. Chen and J. Xu, A novel ultrasound-sensitive mechanofluorochromic AIE-compound with remarkable blue-shifting and enhanced emission, *J. Mater. Chem. C*, 2014, **2**, 5812–5817.

22 X. Zhang, Z. Ma, Y. Yang, X. Zhang, X. Jia and Y. Wei, Fine-tuning the mechanofluorochromic properties of benzothiadiazole-cored cyano-substituted diphenylethene derivatives through D–A effect, *J. Mater. Chem. C*, 2014, **2**, 8932–8938.

23 P. Xue, J. Sun, P. Chen, P. Gong, B. Yao, Z. Zhang, C. Qian, R. Lu and Y. Wei, Strong solid emission and mechanofluorochromism of carbazole-based terephthalate derivatives adjusted by alkyl chains, *J. Mater. Chem. C*, 2015, **3**, 4086–4092.

24 Y. Jiang, D. Cindre, M. Allain, P. Liu, C. Cabanetos and J. Roncali, A mechanofluorochromic push–pull small molecule with aggregation-controlled linear and nonlinear optical properties, *Adv. Mater.*, 2015, **27**, 4285–4289.

25 Y. Zhang, H. Li, G. Zhang, X. Xu, L. Kong, X. Tao, Y. Tian and J. Yang, Aggregation-induced emission enhancement and mechanofluorochromic properties of α-cyanostilbene functionalized tetraphenyl imidazole derivatives, *J. Mater. Chem. C*, 2016, **4**, 2971–2978.

26 T. Nishida, S. Ohta, F. Xu, K. Shinohara, T. Kamada, H. Akashi, M. Takezaki, K. Wakamatsu and A. Orita, Hexafluoroisopropanol as the acid component in the passerini reaction: one-pot access to *β*-amino alcohols, *Org. Lett.*, 2016, **18**, 3988–3991.

27 P. Josse, M. Allain, J. P. Calupitan, Y. Jiang, C. Cabanetos and J. Roncali, Structural control of the molecular packing and dynamics of mechanofluorochromic materials based on small donor–acceptor systems with turn-on luminescence, *Adv. Opt. Mater.*, 2020, **8**, 200420.

28 X. Feng, Y. Chen, Y. Lei, Y. Zhou, W. Gao, M. Liu, X. Huang and H. Wu, Multifunctional properties of a star-shaped triphenylamine-benzene-1,3,5-tricarbohydrazide fluorescent molecule containing multiple flexible chains, *Chem. Commun.*, 2020, **56**, 13638–13641.

29 B. Sarkar, E. Prasad and R. L. Gardas, Systematic photophysical, thermal and electrochemical analysis of a series of phenothiazine cored conjugated aromatic unit appended D–π–A based high-solid state luminescent materials: their applications in reversible mechanofluorochromic and volatile acid sensing, *Mater. Adv.*, 2022, **3**, 2871–2883.

30 B. Prusti, P. Sarkar, S. K. Pati and M. Chakravarty, Multistimuli and fingertip-triggered luminescence switching: a five-colored ink-free rewritable secured platform with strongest red emission, *J. Mater. Chem. C*, 2021, **9**, 9555–9570.

31 X. Zhang, D. Wang, H. Shen, S. Wang, Y. Zhou, Y. Lei, W. Gao, M. Liu, X. Huang and H. Wu, 3,6-Diamino-7,8-dihydroisoquinoline-4-carbonitrile derivatives: unexpected facile synthesis, full-color-tunable solid-state emissions and mechanofluorochromic activities, *Org. Chem. Front.*, 2021, **8**, 856–867.

32 P. Gayathri, M. Pannipara, A. G. Al-Sehemi, D. Moon and S. P. Anthony, Molecular structure controlled self-assembly of pyridine appended fluorophores: multi-stimuli fluorescence responses and fabricating rewritable/self-erasable fluorescent platforms, *Mater. Adv.*, 2021, **2**, 996–1005.

33 F. Xiao, X. Liu, K. Lin, Y. Zhou, W. Gao, Y. Lei, M. Liu, X. Huang and H. Wu, Pyranone−arylbenzene molecules controlled by the competition of local excited state and twisted intramolecular charge-transfer state: dual-state emission, polymorphism, and mechanofluorochromism, *J. Phys. Chem. C*, 2021, **125**, 16792–16802.

34 Y. Wang, I. Zhang, B. Yu, X. Fang, X. Su, Y.-M. Zhang, T. Zhang, B. Yang, M. Li and S. X.-A. Zhang, Full-color tunable mechanofluorochromism and excitation-dependent emissions of single-arm extended tetraphenylethylenes, *J. Mater. Chem. C*, 2015, **3**, 12328–12334.

35 C. Ma, X. Zhang, Y. Yang, Z. Ma, L. Yang, Y. Wu, H. Liu, X. Jia and Y. Wei, Effect of alkyl length dependent crystallinity for the mechanofluorochromic feature of alkyl phenothiazinyl tetraphenylethenyl acrylonitrile derivatives, *J. Mater. Chem. C*, 2016, **4**, 4786–4791.

36 E. Ramachandran and R. Dhamodharan, Tetrakis(trialkylsilylethynylphenyl)ethenes: mechanofluorochromism arising from steric considerations with an unusual crystal structure, *J. Mater. Chem. C*, 2017, **5**, 10469–10476.

37 H. Zhang, Y. Nie, J. Miao, D. Zhang, Y. Li, G. Liu, G. Sun and X. Jiang, Fluorination of the tetraphenylethene core: synthesis, aggregation-induced emission, reversible mechanofluorochromism and thermofluorochromism of fluorinated tetraphenylethene derivatives, *J. Mater. Chem. C*, 2019, **7**, 3306–3314.

38 Q. Yang, D. Li, W. Chi, R. Guo, B. Yan, J. Lan, X. Liu and J. Yin, Regulation of aggregation-induced emission behaviours and mechanofluorochromism of tetraphenylethene through different oxidation states of sulphur moieties, *J. Mater. Chem. C*, 2019, **7**, 8244–8249.

39 Y. Liu, F. X. Lin, Y. Feng, X. Liu, L. Wang, Z.-Q. Yu and B. Z. Tang, Shape-persistent π-conjugated macrocycles with aggregation-induced emission property: synthesis, mechanofluorochromism, and mercury(II) detection, *ACS Appl. Mater. Interfaces*, 2019, **11**, 34232–34240.

40 J. Mei, J. Wang, A. Qin, H. Zhao, W. Yuan, Z. Zhao, H. H. Y. Sung, C. Deng, S. Zhang, I. D. Williams, J. Z. Sun and B. Z. Tang, Construction of soft porous crystal with silole derivative: strategy of framework design, multiple structural transformability and mechanofluorochromism, *J. Mater. Chem.*, 2012, **22**, 4290–4298.

41 K. Amro, A. K. Thakur, M. Rolland, A. V. D. Lee, V. Lemaur, R. Lazzaroni, J. Rault-Berthrlot, C. Poriel, L. Hirsch, S. Clément and P. Gerbier, Linking triptycene to silole: a fruitful association, *Mater. Chem. Front.*, 2020, **4**, 2006–2017.

42 X. Zhang, Z. Chi, H. Li, B. Xu, X. Li, W. Zhou, S. Liu, Y. Zhang and J. Xu, Piezofluorochromism of an aggregation-induced emission compound derived from tetraphenylethylene, *Chem.–Asian J.*, 2011, **6**, 808–811.

43 Y. Dong, B. Xu, J. Zhang, X. Tan, L. Wang, Ji. Chen, H. Lv, S. Wen, B. Li, L. Ye, B. Zou and W. Tian, Piezochromic luminescence based on the molecular aggregation of 9,10-bis((*E*)-2-(pyrid-2-yl)vinyl)anthracene, *Angew. Chem., Int. Ed.*, 2012, **51**, 10782–10785.

44 Y. Liu, Y. Lei, F. Li, J. Chen, M. Liu, X. Huang, W. Gao, H. Wu, J. Ding and Y. Cheng, Indene-1,3-dionemethylene-4*H*-pyran derivatives containing alkoxy chains of various lengths: aggregation-induced emission enhancement, mechanofluorochromic properties and solvent-induced emission changes, *J. Mater. Chem. C*, 2016, **4**, 2862–2870.

45 Y. Wang, D. Xu, H. Gao, Y. Wang, X. Liu, A. Han, C. Zhang and L. Zang, Twisted donor–acceptor cruciform luminophores possessing substituent-dependent properties of aggregation-induced emission and mechanofluorochromism, *J. Phys. Chem. C*, 2018, **122**, 2297–2306.

46 J. Wang, B. Yue, X. Jia, R. Cao, X. Niu, H. Zhao, J. Li and L. Zhu, Mechanical stimuli-induced multiple photophysical responsive AIEgens with high contrast properties, *Chem. Commun.*, 2022, **58**, 3517–3520.

47 Y. Chen, B. Wang, Y. Lei, Y. Zhou, Y. Guo, M. Liu, W. Gao, X. Huang and H. Wu, Stacking-dependent tetracolour luminescence and mechanofluorochromic properties of an isoquinoline derivative with aggregation-induced emission, *Mater. Chem. Front.*, 2022, **6**, 459–465.

48 R. Ding, K. Qin, H. Sun, S. Zhou, S. Guo, H. Feng, H. Ma and Z. Qian, Endowing nitro-compounds with bright and stimuli-responsive luminescence based on propeller-like AIEgens, *J. Mater. Chem. C*, 2021, **9**, 12177–12183.

49 M. A. Potopnyk, M. Kravets, R. Luboradzki, D. Volyniuk, V. Sashuk and J. V. Grazulevicius, Carbazole-modified thiazolo[3,2-c][1,3,5,2]oxadiazaborinines exhibiting aggregation-induced emission and mechanofluorochromism, *Org. Biomol. Chem.*, 2021, **19**, 406–415.

50 F. Khan, A. Ekbote, S. M. Mobin and R. Misra, Mechanochromism and aggregation-induced emission in phenanthroimidazole derivatives: role of positional change of different donors in a multichromophoric assembly, *J. Org. Chem.*, 2021, **86**, 1560–1574.

51 Y. Chen, C. Dai, X. Xu, Y. Zhou, Y. Lei, M. Liu, W. Gao, X. Huang and H. Wu, Effect of connecting units on aggregation-induced emission and mechanofluorochromic properties of isoquinoline derivatives with malononitrile as the terminal group, *J. Phys. Chem. C*, 2021, **125**, 24180–24188.

52 G. Zhang, J. Lu, M. Sabat and C. L. Fraser, Polymorphism and reversible mechanochromic luminescence for solid-state difluoroboron avobenzone, *J. Am. Chem. Soc.*, 2010, **132**, 2160–2162.

53 M. Louis, A. Brosseau, R. Guillot, F. Ito, C. Allain and R. Métivier, Polymorphism, mechanofluorochromism, and photophysical characterization of a carbonyl substituted difluoroboron-*β*-diketone derivative, *J. Phys. Chem. C*, 2017, **121**, 15897–15907.

54 M. Louis, C. P. García, A. Brosseau, C. Allain and R. Métivier, Mechanofluorochromism of a difluoroboron-*β*-diketonate derivative at the nanoscale, *J. Phys. Chem. Lett.*, 2019, **10**, 4758–4762.

55 R. Yoshii, K. Suenaga, K. Tanaka and Y. Chujo, Mechanofluorochromic materials based on aggregation-induced emission-active boron ketoiminates: regulation of the direction of the emission color changes, *Chem.–Eur. J.*, 2015, **21**, 7231–7237.

56 R. P. Nandi, P. Sudhakar, N. K. Kalluvettukuzhy and P. Thilagar, Triarylborane-appended anils and boranils: solid-state emission, mechanofluorochromism, and phosphorescence, *Chem.–Eur. J.*, 2020, **26**, 16306–16317.

57 M. Yamaguchi, S. Ito, A. Hirose, K. Tanaka and Y. Chujo, Modulation of sensitivity to mechanical stimulus in mechanofluorochromic properties by altering substituent positions in solid-state emissive diiodo boron diiminates, *J. Mater. Chem. C*, 2016, **4**, 5314–5319.

58 Z. Zhang, P. Xue, P. Gong, G. Zhang, J. Peng and R. Lu, Mechanofluorochromic behaviors of β-iminoenolate boron complexes functionalized with carbazole, *J. Mater. Chem. C*, 2014, **2**, 9543–9551.

59 Z. Zhang, Z. Wu, J. Sun, B. Yao, G. Zhang, P. Xue and R. Lu, Mechanofluorochromic properties of β-iminoenolate boron complexes tuned by the electronic effects of terminal phenothiazine and phenothiazine-*S,S*-dioxide, *J. Mater. Chem. C*, 2015, **3**, 4921–4932.

60 Z. Zhang, Z. Wu, J. Sun, B. Yao, P. Xue and R. Lu, β-Iminoenolate boron complex with terminal triphenylamine exhibiting polymorphism and mechanofluorochromism, *J. Mater. Chem. C*, 2016, **4**, 2854–2861.

61 B. Poggi, L. Bodelot, M. Louis, R. Métivier and C. Allain, Quantification of mechanofluorochromism at the macroscale via colorimetric analysis of controlled mechanical stimulation, *J. Mater. Chem. C*, 2021, **9**, 12111–12117.

62 B. Tang, M. Li, X. Yu and H. Zhang, Achieving two things at one stroke: crystal engineering simultaneously optimizes the emission and mechanical compliance of organic crystals, *J. Mater. Chem. C*, 2022, **10**, 3894–3900.

63 D. Wang, X. Zhang, X. Han, Y. Zhou, Y. Lei, W. Gao, M. Liu, X. Huang and H. Wu, Ketone–enol tautomerism, polymorphism, mechanofluorochromism and solid-state acidochromism of isoquinolinone–arylidenehydrazine derivatives, *J. Mater. Chem. C*, 2021, **9**, 12868–12876.

64 G. Zhang, J. Tan, L. Zhou, C. Liu, J. Liu, Y. Zou, A. Narita and Y. Hu, S-Shaped double helicene diimides: synthesis, self-assembly, and mechanofluorochromism, *Org. Lett.*, 2021, **23**, 6183–6188.

65 K. Zheng, H. Chen, Y. Xiao, X. Liu, J. Yan and N. Zhang, A novel strategy to design and construct aie-active mechanofluorochromic materials via regulation of molecular structure, *Chem.–Eur. J.*, 2021, **27**, 14964–14970.

66 M. Okazaki, Y. Takeda, P. Data, P. Pander, H. Higginbotham, A. P. Monkman and S. Minakata, Thermally activated delayed fluorescent phenothiazine–dibenzo[a,j]phenazine–phenothiazine triads exhibiting tricolor-changing mechanochromic luminescence, *Chem. Sci.*, 2017, **8**, 2677–2686.

67 S. Mizukami, H. Houjou, K. Sugaya, E. Koyama, H. Tokuhisa, T. Sasaki and M. Kanesato, Fluorescence color modulation by intramolecular and intermolecular π-π interactions in a helical zinc(II) complex, *Chem. Mater.*, 2005, **17**, 50–56.

68 V. Kozhevnikov, B. Donnio and D. Bruce, Phosphorescent, terdentate, liquid-crystalline complexes of platinum(II): stimulus-dependent emission, *Angew. Chem., Int. Ed.*, 2008, **47**, 6286–6289.

69 E. Szerb, A. Talarico, I. Aiello, A. Crispini, N. Godbert, D. Pucci, T. Pugliese and M. Ghedini, Red to green switch driven by order in an ionic Ir^{III} liquid-crystalline complex, *Eur. J. Inorg. Chem.*, 2010, 3270–3277.

70 Y. Ai, Y. Li, M. H.-Y. Chan, G. Xiao, B. Zou and V. W.-W. Yam, Realization of distinct mechano- and piezochromic behaviors via alkoxy chain length-modulated phosphorescent properties and multidimensional self-assembly structures of dinuclear platinum(II) complexes, *J. Am. Chem. Soc.*, 2021, **143**, 10659–10667.

71 H. Langhals, T. Potrawa, H. Nöth and G. Linti, The influence of packing effects on the solid-state fluorescence of diketopyrrolopyrroles, *Angew. Chem., Int. Ed. Engl.*, 1989, **28**, 478–480.

72 H.-C. Yeh, W.-C. Wu, Y.-S. Wen, D.-C. Dai, J.-K. Wang and C.-T. Chen, Derivative of α,β-dicyanostilbene: convenient precursor for the synthesis of diphenylmaleimide compounds, *E*−*Z* isomerization, crystal structure, and solid-state fluorescence, *J. Org. Chem.*, 2004, **69**, 6455–6462.

73 Y. Ooyama, T. Okamoto, T. Yamaguchi, T. Suzuki, A. Hayashi and K. Yoshida, Heterocyclic quinol-type fluorophores: synthesis, x-ray crystal structures, and solid-state photophysical properties of novel 5-hydroxy-5-substituent-benzo[*b*]naphtho[1,2-*d*]furan-6-one and 3-hydroxy-3-substituent-benzo[*kl*]xanthen-2-one derivatives, *Chem.–Eur. J.*, 2006, **12**, 7827–7838.

74 T. Nakae, M. Nishio, T. Usuki, M. Ikeya, C. Nishimoto, S. Ito, H. Nishihara, M. Hattori, S. Hayashi, T. Yamada and Y. Yamanoi, Luminescent Behavior Elucidation of a Disilane-Bridged D–A–D Triad Composed of Phenothiazine and Thienopyrazine, *Angew. Chem., Int. Ed.*, 2021, **60**, 22871–22878.

75 K. Imato, T. Enoki, K. Uenaka and Y. Ooyama, Synthesis and photophysical and electrochemical properties of pyridine-, pyrazine- and triazine-based $(D\text{-}\pi\text{-})_2A$ fluorescent dyes, *Beilstein J. Org. Chem.*, 2019, **15**, 1712–1721.

76 E. Lippert, Dipolmoment und elektronenstruktur von angeregten molekülen, *Z. Naturforsch.*, 1955, **10**, 541–545.

77 N. Mataga, Y. Kaifu and M. Koizumi, Solvent effects upon fluorescence spectra and the dipolemoments of excited molecules, *Bull. Chem. Soc. Jpn.*, 1956, **29**, 465–470.

78 C. Reichardt, *Solvents and Solvent Effects in Organic Chemistry*, VCH, Weinheim, 2003.

79 S. Sumalekshmy and K. R. Gopidas, Intramolecular charge transfer processes in donor–acceptor substituted vinyltetrahydropyrenes, *Photochem. Photobiol. Sci.*, 2005, **4**, 539–546.

80 F. B. Dias, S. Pollock, G. Hedley, L.-O. Pålsson, A. Monkman, I. I. Perepichka, I. F. Perepichka, M. Tavasli and M. R. Bryce, Intramolecular charge transfer assisted by conformational changes in the excited state of fluorene-dibenzothiophene-*S,S*-dioxide co-oligomers, *J. Phys. Chem. B*, 2006, **110**, 19329–19339.

81 G.-J. Zhao, R.-K. Chen, M.-T. Sun, J.-Y. Liu, G.-Y. Li, Y.-L. Gao, K.-L. Han, X.-C. Yang and L. Sun, Photoinduced

intramolecular charge transfer and S_2 fluorescence in thiophene-π-conjugated donor–acceptor systems: experimental and TDDFT studies, *Chem.–Eur. J.*, 2008, **14**, 6935–6947.

82 R. S. Butler, P. Cohn, P. Tenzel, K. A. Abboud and R. K. Castellano, Synthesis, photophysical behavior, and electronic structure of push−pull purines, *J. Am. Chem. Soc.*, 2009, **131**, 623–633.

83 Y. Ooyama, G. Ito, K. Kushimoto, K. Komaguchi, I. Imae and Y. Harima, Synthesis and fluorescence and electrochemical properties of D–π-A structural isomers of benzofuro[2,3-*c*]oxazolo[4,5-*a*]carbazole-type and benzofuro[2,3-*c*]oxazolo[5,4-*a*]carbazole-type fluorescent dyes, *Org. Biomol. Chem.*, 2010, **8**, 2756–2770.

84 T. Enoki, K. Matsuo, J. Ohshita and Y. Ooyama, Synthesis and optical and electrochemical properties of julolidine-structured pyrido[3,4-*b*]indole dye, *Phys. Chem. Chem. Phys.*, 2017, **19**, 3565–3574.